The solution structure of the pH-induced monomer of dynein light-chain LC8 from *Drosophila*

MOSES MAKOKHA,[1] YUANPENG JANET HUANG,[2] GAETANO MONTELIONE,[2] ARTHUR S. EDISON,[3] AND ELISAR BARBAR[1,4]

[1]Department of Chemistry and Biochemistry, Ohio University, Athens, Ohio 45701-2979, USA
[2]Center for Advanced Biotechnology and Medicine, Department of Molecular Biology and Biochemistry, Rutgers University, Piscataway, New Jersey 08854, USA
[3]Department of Biochemistry and Molecular Biology, University of Florida, Gainesville, Florida 32610-0245, USA

(RECEIVED September 28, 2003; FINAL REVISION November 14, 2003; ACCEPTED November 17, 2003)

Abstract

The structure of *Drosophila* LC8 pH-induced monomer has been determined by NMR spectroscopy using the program AutoStructure. The structure at pH 3 and 30°C is similar to the individual subunits of mammalian LC8 dimer with the exception that a β strand, which crosses between monomers to form an intersubunit β-sheet in the dimer, is a flexible loop with turnlike conformations in the monomer. Increased flexibility in the interface region relative to the rest of the protein is confirmed by dynamic measurements based on ^{15}N relaxation. Comparison of the monomer and dimer structures indicates that LC8 is not a domain swapped dimer.

Keywords: domain swapping; protein structure; dimerization; dynein light chain; pH-induced dissociation

LC8, a 10-kD light-chain subunit of cytoplasmic dynein, has an unusually high degree of sequence homology among species. *Drosophila* LC8 is 94%, 71%, and 50% identical with LC8 from human, *Aspergillus nidulans*, and yeast, respectively. LC8 is present in all functional dyneins and is presumed to have a fundamental role in the regulation and assembly of the motor complex. LC8 forms a tight subcomplex with light-chain Tctex-1 and intermediate-chain IC74 (King et al. 1998; Makokha et al. 2002). In this interaction, LC8 binding promotes the assembly of the complex by increasing the structure of the intrinsically unfolded N-terminal domain of IC74 (Makokha et al. 2002; Nyarko et al. 2003). The LC8 subunit is present in myosin V (Espindola et al. 2000) and may serve a similar function in the assembly of its dimeric heavy-chain motor subunits and in actin-based vesicle transport (Naisbitt et al. 2000). LC8 is also presumed to target dynein to cellular cargo, because it interacts with several proteins with unrelated functions. For example, human LC8 interacts with neuronal nitric oxide synthase (nNOS) either to inhibit its activity (Jaffrey and Snyder 1996) or to facilitate its transport along the microtubules within axons (Rodriguez-Crespo et al. 1998). In vertebrates, LC8 interacts with IκBα (Crepieux et al. 1997) and with a pro-apoptotic protein, bim (Puthalakath et al. 1999). LC8 also binds to several viruses including rabies virus P protein and lyssavirus phosphoprotein, indicating that it is involved in directly transporting viruses along microtubules on entry to the cell (Jacob et al. 2000; Raux et al. 2000). In *Drosophila*, LC8 interacts with the Swallow protein, a protein that colocalizes with bicoid mRNA during oogenesis, and may act as an adapter to enable dynein to transport mRNA along microtubules (Schnorrer et al. 2000).

LC8 is a tight dimer in human and rat (Liang et al. 1999; Fan et al. 2001), a moderately tight dimer in *Drosophila* (Kd 12μM), and primarily a stable monomer in *A. nidulans* (Barbar et al. 2001b). The crystal structure of LC8 dimer from human (Liang et al. 1999) and an NMR structure from rat (Fan et al. 2001) show that each monomer comprises five contiguous β strands and two helices (Fig. 1), and that

Reprint requests to: Elisar Barbar, Department of Biochemistry and Biophysics, Oregon State University, Corvallis, OR 97331, USA; e-mail: barbare@science.oregonstate.edu; fax: (541) 737-0481.
[4]Present address: Department of Biochemistry and Biophysics, Oregon State University, Corvallis, OR 97331, USA.

Article published online ahead of print. Article and publication date are at http://www.proteinscience.org/cgi/doi/10.1110/ps.03462204.

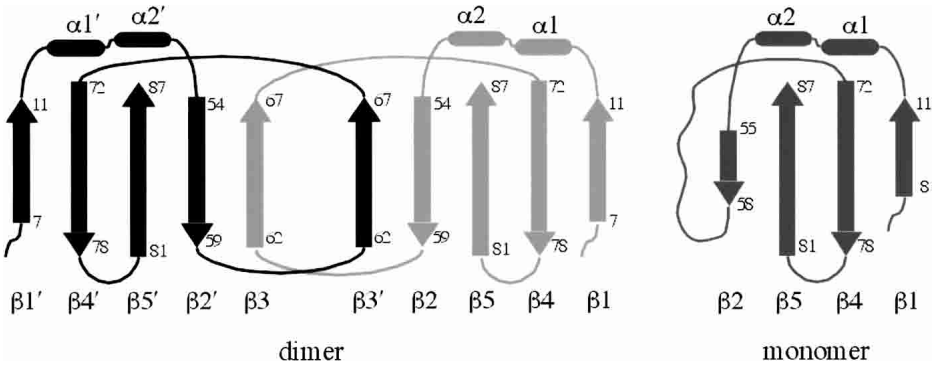

Figure 1. Comparison of LC8 topology in the dimer (gray and black) and monomer (dark gray). The notation of the dimeric structure (Liang et al. 1999) is used in naming the β strands.

dimerization involves a β3–β2′ interaction. One question raised by the dimer structure is the disposition of the primarily hydrophobic "orphan" β3 strand upon dissociation and separation from the β2′ strand (Liang et al. 1999). An interesting possibility is suggested by an early NMR structure of LC8 (Tochio et al. 1998). It was reported that LC8 is a monomer with an intramolecular β3–β2 interaction, but later work showed that the data were instead consistent with a dimeric structure (Fan et al. 2001). Although the conclusion that LC8 is a monomer at neutral pH was later proven to be incorrect (Barbar et al. 2001b), the initial report of a β3–β2 interaction in an LC8 monomer raised the possibility of domain swapping (Fan et al. 2001) in the formation of the dimer. Recently, LC8 was described as a nonconventional domain swapped dimer, based on comparison of the structure of the dimer with the structure of pH-induced monomer from rat (Wang et al. 2003).

We have previously shown that *Drosophila* LC8 is a moderately tight dimer at neutral pH but dissociates to a folded monomer at pH <4.5 (Barbar et al. 2001b). We characterized the pH dependence of dissociation by using a series of sedimentation equilibrium experiments. The resulting sigmoidal curve with a midpoint of ~4.8 indicated that dissociation arises from titration of a group with pKa ~4.8. In the pH range 2.5–8.5, LC8 retains native average secondary and tertiary structure as monitored by fluorescence and circular dichroism spectroscopy. Other than lowered pH, conditions that favor the monomer include low protein concentration (<0.5 μM) and the presence of 1–2.5 M GdnCl. Based on the moderately tight dimerization constant and the folded structure of the monomer, we proposed a relationship between LC8 monomer–dimer equilibrium and function (Barbar et al. 2001b). Elucidating the structure of LC8 monomer is one step in testing this hypothesis.

Here, we report the NMR structure of pH-induced LC8 monomer from *Drosophila* at pH 3, along with mobility data using partly automated methods for resonance assignments and structural determination. Although the structure is similar to the low-pH monomer structure in rat, we argue that LC8 dimer (from either species) should not be classified as domain swapped.

Results

Resonance assignments and secondary structure analysis

Ninety-five percent of backbone resonance assignments and 85% of side-chain assignments for monomeric LC8 at pH 3 were obtained from the combined use of automated and manual analysis of triple-resonance NMR spectra. Figure 2 shows the medium- and short-range NOEs used for secondary structure determination, residues exhibiting slow amide proton exchange, and $^3J(H^N\text{-}H^\alpha)$ scalar coupling constants. Amide protons are considered slowly exchanging and are indicated by a diamond if they have a rate constant $<0.88 \times 10^{-3}$ min^{-1} at pH 3.0 and 30°C. $^3J(H^N\text{-}H^\alpha)$ scalar coupling constants <4 Hz (indicative of helical structure), and >8 Hz (β strand), and between 4 and 8 Hz, are indicated by open circles, filled circles, and semicircles, respectively.

Structure determination

The structure of *Drosophila* LC8 monomer was determined at pH 3 in a fully automated iterative manner by using the NOESY analysis program AutoStructure (Huang et al. 2003). A total of 1129 conformation-restricting constraints were identified. These include 939 NOE distance constraints, 122 dihedral constraints, and 68 hydrogen bond constraints (two per hydrogen bond). The root mean square deviations for backbone and all heavy atoms in this ensemble of structures are 0.4 Å and 0.9 Å for ordered residues and 1.0 Å and 1.5 Å for all residues. A summary of the distributions of the resulting constraints is presented in Table 1. The solution NMR structure generated from these constraints is represented by the set of 10 out of 56 struc-

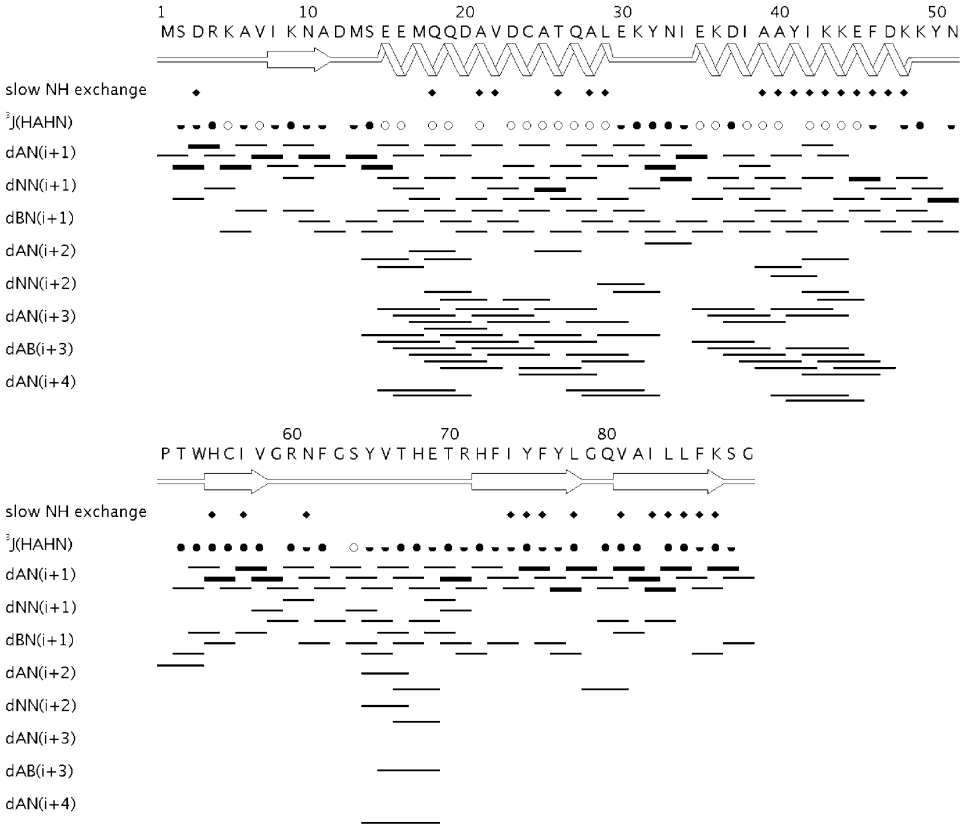

Figure 2. Sequential connectivity diagram showing medium- and short-range NOEs. Residues with slowly exchanging backbone amide protons are represented by filled diamonds, and coupling constants are grouped as <6 Hz (open circles) for helical structure, >8 Hz (filled circles) for β strand, and between 6 Hz and 8 Hz (filled semicircles) for coil. Interresidue NOE connectivities are shown as thin, medium, and thick black lines, corresponding to weak, medium, and strong NOE interactions, respectively. The image was generated with the Assignment Validation Suite software (Moseley et al. 2003). All NMR data were collected on pH 3.0 samples at 30°C.

tures with lowest values of the DYANA target function (Fig. 3). Figure 3 shows a stereo view of the ensemble of NMR structures, along with a ribbon diagram of the lowest-energy structure generated by MOLMOL (Koradi et al. 1996). These structures exhibit no violations of the NOE-based distance constraints >0.5 Å, no violations of dihedral constraints >10 degrees, and no violations of steric constraints >0.5 Å (Table 1).

LC8 monomer is a mixed α/β protein. There are two α helices, α1 (15–29), and α2 (35–48). These two helices are slightly shorter than the corresponding α1 (15–31), and α2 (35–50) helices of dimer LC8 from rat (100% sequence identity with human; Fan et al. 2001). There are four β strands: β1 (8–11), β2 (55–58), β4 (72–78), and β5 (81–87; Fig. 1). In naming the β strands, we use the notation of the dimeric structure of human LC8 (Liang et al. 1999). Strand β1 is shorter and more flexible than that of the dimer. Strand β2 is shorter than the corresponding strand in the dimer structure (55–58 versus 54–59), but it is packed against strand β5, as it is in the dimer. Antiparallel strands β4 and β5 are not perturbed in the monomer. Slow-exchanging amide protons in α2 and β5 (Fig. 2) indicate that these segments are buried and form the core of the monomeric protein.

Several poorly defined regions indicative of structural disorder are present in the monomer, including N-terminal residues 1–7, C-terminal residues 88–89, the short loops between β1 and α1 and between α2 and β2, and residues 62–69 connecting β2 to β4. Residues 62–67, which correspond to β3 in the dimer, are a loop with turnlike conformations in equilibrium with more disordered conformations. The turnlike conformations of this loop are inferred from a set of weak medium-range NOEs: $d_{\alpha N}(i+4)$ between Tyr65 and Glu69, $d_{NN}(i+3)$ between Tyr65 and His68, and $d_{\alpha N}(i+3)$ between Val66 and Glu69 (Fig. 2). Flexibility in residues 62–67 is inferred from fast amide proton exchange rates, as well as $^3J(H^N\text{-}H^\alpha)$ scalar coupling constants indicative of disordered conformations. The absence of long-range NOEs for this segment indicates that it is not packed against other elements of the structure.

Table 1. *Summary of spectral and structural statistics for* Drosophila *LC8 monomer ensemble of the 10 lowest-energy structures*

NOESY spectral data	N15	C13
Number of peaks	537	2116
Number of "assignable" peaks	496	1571
Number of peak assignments	446	1372
Completeness of resonance assignments (%)		
Assignable backbone atoms		95
All assignable atoms		85
Summary of conformationally-restricting constraints derived by AutoStructure		
Distance constraints		
Total		939
Intra-residue (i = j)		102
Sequential (|i–j| = 1)		240
Medium range (1<|i–j|≤5)		240
Long range (|i–j|>5)		357
Dihedral angle constraints		122
Hydrogen bond constraints		68
Long range		20
Total number of constraints		1129
Number of constraints per residue		13.8
Long range constraints per residue		4.2
Root mean square deviation (Å)[a]		
Backbone atoms		0.4
All heavy atoms		0.9
Residual constraint violations		
Distance violations[b]		
0.1–0.2 Å		12.7
0.2–0.5 Å		1.9
>0.5 Å		0
Average violation (Å)		0.02
Maximum violation (Å)		0.37
Van der Waals violations[c]		
0.1–0.2 Å		0.5
0.2–0.5 Å		1.8
> 0.5 Å		0
Average violation (Å)		0.16
Maximum violation (Å)		0.22
Dihedral angle violations[b]		
1–10°		8.4
>10°		0
Average violation (degrees)		0.70
Maximum violation (degrees)		7.5
ProCheck analysis of dihedral angles[a]		
Most favored regions (%)		73.6
Additional allowed (%)		23.6
Generously allowed (%)		2.8
Disallowed (%)		0.0
G-score (ϕ,ψ)		–0.94
G-score (all dihedrals)		–1.12

[a] Residues 8–10, 14–49, 52–58, 60–61, 66–68, and 70–87 (with sum of ϕ and ψ order parameters >1.8) were used in the Procheck (Laskowski et al. 1996) analysis and root mean square deviation values calculations.
[b] Distance violations within ranges 0.1–0.2, 0.2–0.5, and >0.5 Å and dihedral angle violations within ranges 1–10 and >10° are reported as the average of the number of violations for each model in each of these bins.
[c] Van der Waals violations within ranges 0.1–0.2, 0.2–0.5, and >0.5 Å were the average violation in all models in each of these bins.

Backbone dynamics

Backbone ^{15}N relaxation rates were measured for LC8 monomer under the same conditions at which the structure was solved. Values of heteronuclear ^{15}N-^{1}H NOEs, ^{15}N relaxation rates (R_2, and R_1), are plotted as a function of residue number in Figure 4. The high R_2 values of two residues most probably arise from exchange broadening. The N-terminal residues 2–6 show negative heteronuclear ^{15}N-^{1}H NOEs and low R_1 values, indicating a high degree of conformational disorder. Residues 60–72 have smaller positive NOEs relative to the rest of the molecule. The average magnitude of the heteronuclear NOEs in this segment, only 0.4 units, together with smaller R_1 values in the same segment, is evidence of dynamic flexibility. Interestingly, the overall orientation of this flexible segment relative to the rest of the molecule is not greatly different in the monomer and dimer (Fig. 5A). The disordered loop in the monomer (pink) substantially overlays with the β3 strand in the dimer (blue and green).

Discussion

We have previously determined that LC8 at pH 3 is a folded and compact monomer, with CD-detected structure similar to the dimer at pH 7 (Barbar et al. 2001b). Fluorescence emission spectra at both pHs are also similar, indicating that the tertiary packing in the environment of the single Trp, Trp 54, is not perturbed upon dissociation. The monomer at pH 3 shows remarkable stability and has cooperative chemical and thermal denaturation profiles, indicating that it still has a compact core similar to the dimer at pH 7. The high-resolution monomeric structure determined in this work confirms that the monomer is compact and similar to the dimer of mammalian LC8 except that β3 of the dimer becomes a disordered loop with turnlike conformations in the monomer. In addition, there is an increase in dynamic flexibility in segments at the N terminus and at the interface region, which we have confirmed by ^{15}N relaxation studies.

Solvent-accessible surface areas were measured for an ensemble of the 10 lowest-energy structures for monomeric LC8 and compared with the ensemble of 10 lowest-energy structures of one subunit of the dimer of LC8 from rat (Fan et al. 2001). Solvent-accessible surface areas for the LC8 monomer are greater than those calculated for each subunit of the dimer by 1000 ± 200 Å^2. Interface residues 60–72 contribute 250 ± 80 Å^2, and the completely disordered residues 1–6 contribute 210 ± 90 Å^2. This increase in solvent accessibility in these segments relative to the rest of the protein is consistent with an increase in flexibility and fewer intramolecular contacts in the monomer compared with the corresponding segments of one subunit of the dimer (Jones and Thornton 1995).

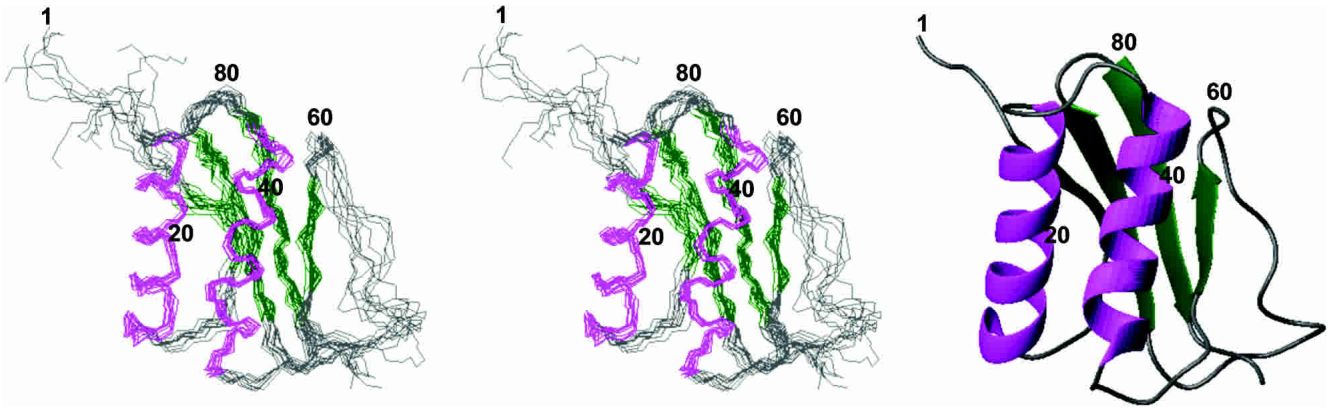

Figure 3. Solution structures of monomeric *Drosophila* LC8. Stereo view of the ensemble of the 10 lowest-energy structures with every 20th residue labeled (*left*), along with a ribbon diagram of the lowest-energy structure (*right*) generated by MOLMOL.

The LC8 dimer structure (Liang et al. 1999; Fan et al. 2001) shows that His55 and 55′ in β2 and β2′ at the dimer interface are separated by 6Å (Fig. 5B). We have suggested that dissociation of the dimer at low pH is due to protonation of this residue, which creates a repulsive interaction between groups buried in the dimer interface (Barbar et al. 2001b). The hydrophobic environment of His55 in the dimer is primarily due to quaternary interactions with β3′ across the interface (Fig. 5B) because the His55 side chain is completely buried in the dimer, somewhat solvent-exposed in one subunit of dimer, and more exposed in the pH 3 monomer. His55 is also packed against residues Phe86 and Ser88 of β5 in both the dimer and monomer (Fig. 5A). Although the solvent-accessible surface area of His55 is somewhat increased in the monomer relative to one subunit of dimer, the solvent-accessible surface areas of Phe86 and Ser88 side chains do not change, indicating that their packing against His55 in the monomer is not perturbed at low pH. Figure 5A shows an overlay of side chains Lys43, Trp54, Phe86, and Ser88, which are in close proximity to His55. The packing of these residues is not significantly changed in the pH 3 monomer. Taken together, these results are consistent with the hypothesis that His55 protonation drives dimer dissociation at low pH but does not further destabilize the structure of the monomer.

The dissociation of LC8 to a stable monomer is in keeping with the concept of negative protein design (Richardson and Richardson 2002). The β-sheet of each subunit in LC8 dimer has two edge strands, β1 and β3 (Fig. 1). In β1, a β-bulge is present in both monomer and dimer, which disfavors further β strand interactions by providing a local outward protrusion. Strand β3 in the dimer is ideally suited for edge-to-edge aggregation because it is highly hydrophobic and extended. Upon low pH dissociation, which we propose is coupled to His55 protonation, the resulting structure has β3 and part of β2 in an irregular conformation

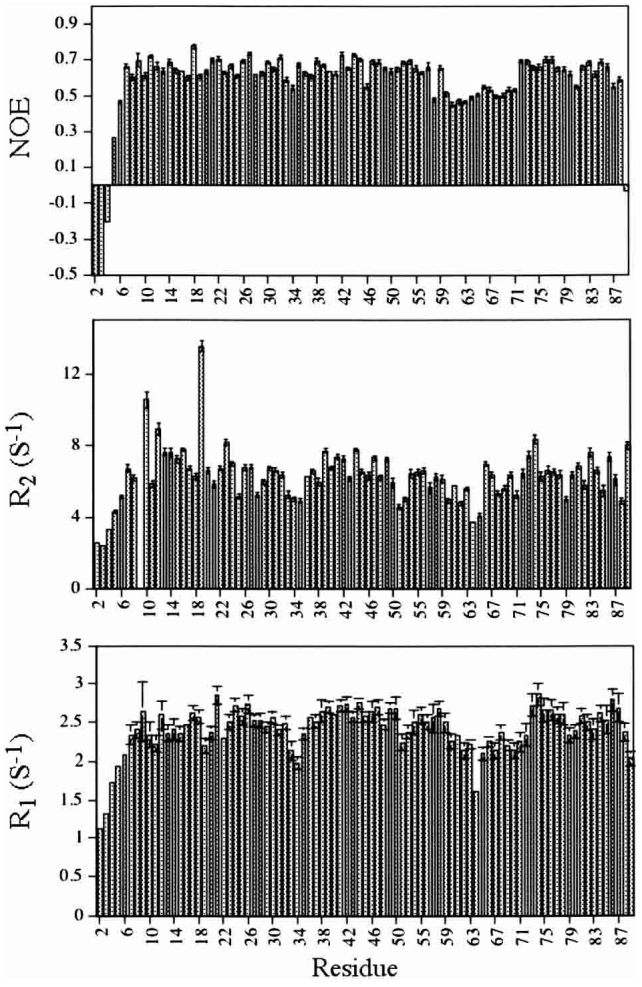

Figure 4. NMR relaxation data that identify regions of structure and mobility. Plots of ^{15}N R_1 and R_2 and steady-state ^{15}N-^{1}H NOE are recorded for monomeric LC8 at pH 3.0 and 30°C. The data show that residues 2–6 are highly disordered, and residues 60–72 are more mobile than is the rest of the molecule.

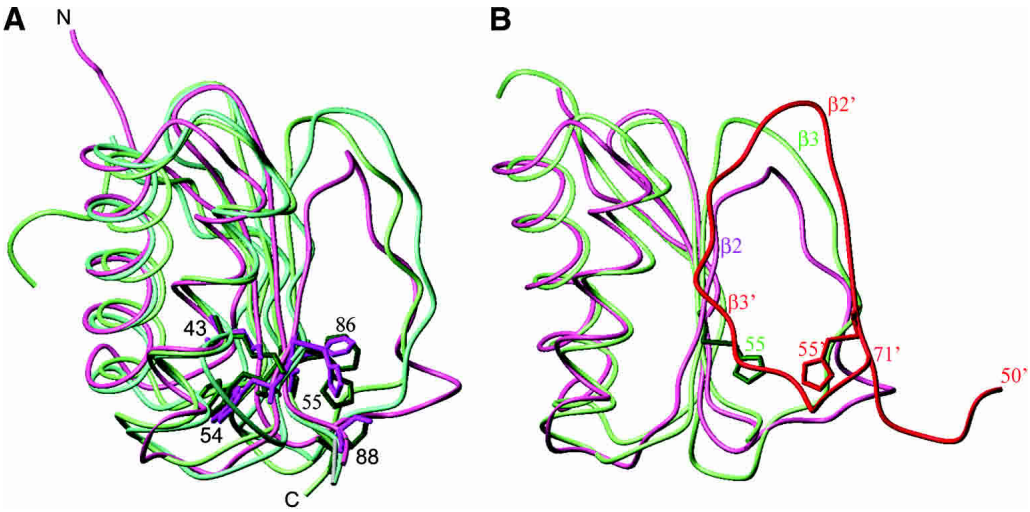

Figure 5. (*A*) Overlay of backbone monomeric LC8 (pink) and subunit A of dimeric mammalian LC8 determined from crystallography (blue) and NMR (green). The residues that exhibit poor backbone alignment are 60–71 and 1–8. Side chains His55, Trp54, Lys43, Phe86, and Ser88 are shown in purple for LC8 monomer and green for subunit A of LC8 dimer. (*B*) Overlay of backbone monomeric LC8 (pink) and one subunit of dimeric rat LC8 (green). A segment of the second subunit in the dimer showing strands β2′ and β3′ is given in red. Side chain His55 is ~6 Å apart from His55′.

unsuitable for β-sheet interactions. In the low pH structure, the presence of a charged side chain and the change of a strand to a loop is consistent with negative design by which β-sheet proteins avoid edge-to edge aggregation and favor monomeric structures.

It has been reported (Fan et al. 2001; Wang et al. 2003) that the dimer structure of LC8 is formed by domain swapping (Schlunegger et al. 1997). Domain swapping provides an efficient mechanism for the genesis of dimer from stable monomers, but other mechanisms for the formation of intertwined dimers are known (Xu et al. 1998). The term domain swapping should properly be restricted to those cases in which, in the words of Schlunegger et al. (1997), "the swapped domain has nearly identical noncovalent interactions in the oligomer as in the monomer." If LC8 is a domain swapped dimer, the intertwined β3 strand should make nearly identical noncovalent interactions with β2′ in the dimer as with β2 in the monomer. In LC8 pH-induced monomer, β3 is replaced by a flexible loop with turnlike conformations that overlays well with β3 of the dimer and is not shifted closer to β2 of the monomer structure. This is illustrated in Figure 5B, in which β3′ and β2′ of the other subunit are shown in red. The structure therefore argues against a three-dimensional (3D) domain swapping hypothesis for dimer formation, because the β3–β2′ contacts of the dimer are not replicated in analogous β3–β2 contacts in the monomer.

Materials and methods

Protein preparation

The cDNA for LC8 was subcloned into a pET-15D vector and expressed in *Escherichia coli* BL21(DE3) cell lines as a His-tag fusion protein. Uniformly ^{15}N and $^{15}N/^{13}C$ isotopically labeled protein were prepared by growing the bacteria in MJ9 media containing 1 g/L of $^{15}NH_4CL$ and 2 g /L of ^{12}C or ^{13}C glucose. The cells were grown at 37°C to an OD_{600} of 0.6, and protein expression was induced with 0.2 mM isopropyl D-thiogalactoside (IPTG) for 4 h at 27°C. The cells were harvested by centrifugation and lysed by sonication. Recombinant LC8 was purified by affinity chromatography using Ni^{2+}-NTA column (Qiagen). The 6×His-tag was removed by treatment with Factor Xa for 12 h at 37°C. The cleaved protein was further purified by ion exchange chromatography using High Q column (Bio Rad). All NMR spectra were collected by using samples containing 0.8 to 1.4 mM LC8 protein, 50 mM citrate phosphate (pH 3), 50 mM NaCl, 1 mM sodium azide, 10% D_2O, and 3% glycerol. Purity of >95% was verified by SDS-PAGE and analytical size exclusion chromatography.

NMR spectroscopy

All NMR spectra used in the structure determination of monomeric LC8 were collected at 30°C on a 600-MHz Bruker DMX spectrometer except where indicated. Spectra were processed by using the program Felix 97 (Accelerys) and NMRPipe (Delaglio et al. 1995).

For resonance assignments, the majority of backbone resonance assignments were determined by using the program AutoAssign (Zimmerman et al. 1997). The input for AutoAssign included peak lists from two-dimensional (2D) ^1H-^{15}N HSQC and 3D HNCO, CBCANH, and CBCAcoNH (Grzesiek and Bax 1992; Muhandiram and Kay 1994). Results obtained from automated assignments were extended by manual analysis of experiments for side-chain assignments, which include 3D HCCH-TOCSY (Clore and Gronenborn 1994), hCCcoNH-TOCSY and HcccoNH-TOCSY (Grzesiek et al. 1993; Muhandiram and Kay 1994). Side-chain aromatic ^1H and ^{13}C resonance assignments were made using homonuclear 2D TOCSY, COSY, NOESY, and ^1H and ^{13}C CT-HSQC acquired after lyophilizing the protein from water and dissolving it in D_2O.

The spectra used in deriving distance constraints included 3D ^{15}N, ^{13}C, and simultaneously edited NOESY (mixing time of 140 msec) recorded at 750 MHz (Pascal et al. 1994). Coupling constants $^{3}J(H^{N}\text{-}H^{\alpha})$ were obtained from 3D HNHA experiment (Kuboniwa et al. 1994). Amide hydrogen exchange rates were determined by dissolving the lyophilized protein in D_2O, and acquiring a series of 2D $^{1}H\text{-}^{15}N$ HSQC spectra in the interval of 20 min to 1 week.

The 3D structure of LC8 was determined first in a fully automated iterative manner by using the NOESY analysis program AutoStructure (Greenfield et al. 2001; Huang et al. 2003) together with structure generation program DYANA (Guntert et al. 1997) and was then refined with manual analysis. AutoStructure is a rule-based expert system, which automatically interprets NOE cross peaks based on the identification of self-consistent NOE contact pattern. The experimental NMR data used for AutoStructure analysis included the resonance assignment list, NOESY peak lists derived from the 3D ^{15}N-edited and ^{13}C-edited NOESY data, $^{3}J(H^{N}\text{-}H^{\alpha})$ scalar coupling constants, and slow amide exchange data. Lists of all possible assignments were generated from the NOESY peak lists with frequency match tolerance of 0.05 ppm for ^{1}H and 0.5 ppm for ^{15}N and ^{13}C dimensions. Hydrogen bonds were identified by AutoStructure based on combined analysis of NOESY constraint patterns and amide proton exchange rates. Dihedral angle constraints were determined by combined analysis of chemical shift, $^{3}J(H^{N}\text{-}H^{\alpha})$ scalar coupling, and NOESY data.

Relaxation measurements

T_1, T_2, and heteronuclear NOE experiments were acquired at 30°C at 500 MHz by using pulse sequences as in Barbar et al. (2001a). Values of R_1 were determined from 11 spectra with relaxation delays ranging from 0.05 to 1 sec, with 64 scans per increment and 1.7 sec for recycle delay. Values of R_2 were determined from nine spectra with relaxation delays ranging from 0.01 to 0.23 sec, with 64 scans per increment and 1.9 sec for recycle delay. Steady-state $^{1}H\text{-}^{15}N$ NOEs were determined from pairs of spectra recorded in the presence and absence of amide proton saturation with 128 increments of 192 scans each. Spectra recorded with proton saturation used a 3-sec period of saturation and an additional 1-sec delay, whereas those recorded in the absence of proton saturation were acquired with a 4-sec relaxation delay. Saturation was achieved by the application of a train of 90-degree pulses separated by 5-msec delay.

Values of relaxation time constants, T_1 and T_2, were determined by fitting the measured peak height versus time profiles to a single exponential decay function $I_t = I_0 \exp(-t/T)$, where t is the variable relaxation delay, I_t is the intensity measured at time t, and I_0 is the intensity at time zero. Uncertainties in the relaxation times were determined from standard error in the slope of the linear fit of the natural log of I_t versus time. NOE values reported are the average of ratios of peak intensities in the presence and absence of proton saturation obtained from duplicate experiments. Relaxation data analysis and curve fitting were obtained by using Art Palmer's suite of programs (Columbia University). Solvent-accessible surface areas were measured by using algorithms based on α shapes (Liang et al. 1998).

Protein Data Bank and BioMagRes Database accession number

The structural coordinates are deposited with the RCSB Protein Data Bank (PDB) and assigned a PDB ID of 1RHW. The chemical shifts are assigned a BioMagRes ID of BMRB-8998.

Acknowledgments

We appreciate the assistance of Nancy Isern at the Pacific National Laboratory and Dr. In Ja Byeon at the Ohio NMR consortium. Other NMR data were collected at the AMRIS facility at the University of Florida. This work is supported by NIH grant GM60969 and NSF CAREER grant MCB-0238094 to E.B., and the National High Magnetic Field Laboratory (NHMFL) external user program.

The publication costs of this article were defrayed in part by payment of page charges. This article must therefore be hereby marked "advertisement" in accordance with 18 USC section 1734 solely to indicate this fact.

References

Barbar, E., Hare, M., Makokha, M., Barany, G., and Woodward, C. 2001a. NMR-detected order in core residues of denatured bovine pancreatic trypsin inhibitor. *Biochemistry* **40:** 9734–9742.

Barbar, E., Kleinman, B., Imhoff, D., Li, M., Hays, T., and Hare, M. 2001b. Dimerization and folding of LC8, a highly conserved light chain of cytoplasmic dynein. *Biochemistry* **40:** 1596–1605.

Clore, G.M. and Gronenborn, A.M. 1994. Multidimensional heteronuclear nuclear magnetic resonance of proteins. In *Nuclear magnetic resonance*, Part C. (eds. T.L. James and N.J. Oppenheimer), pp. 349–363. Academic Press, San Diego, CA.

Crepieux, P., Kwon, H., Leclerc, N., Spencer, W., Richard, S., Lin, R.T., and Hiscott, J. 1997. IκBα physically interacts with a cytoskeleton-associated protein through its signal response domain. *Mol. Cell. Biol.* **17:** 7375–7385.

Delaglio, F., Grzesiek, S., Vuister, G.W., Zhu, G., Pfeifer, J., and Bax, A. 1995. NMRpipe: A multidimensional spectral processing system based on Unix pipes. *J. Biomol. NMR* **6:** 277–293.

Espindola, F.S., Suter, D.M., Partata, L.B.E., Cao, T., Wolenski, J.S., Cheney, R.E., King, S.M., and Mooseker, M.S. 2000. The light chain composition of chicken brain myosin-Va: Calmodulin, myosin-II essential light chains, and 8-kDa dynein light chain/PIN. *Cell Motil. Cytoskeleton* **47:** 269–281.

Fan, J.S., Zhang, Q., Tochio, H., Li, M., and Zhang, M.J. 2001. Structural basis of diverse sequence-dependent target recognition by the 8 kDa dynein light chain. *J. Mol. Biol.* **306:** 97–108.

Greenfield, N.J., Huang, Y.J., Palm, T., Swapna, G.V.T., Monleon, D., Montelione, G.T., and Hitchcock-DeGregori, S.E. 2001. Solution NMR structure and folding dynamics of the N terminus of a rat non-muscle α-tropomyosin in an engineered chimeric protein. *J. Mol. Biol.* **312:** 833–847.

Grzesiek, S., and Bax, A. 1992. Improved 3D triple-resonance NMR techniques applied to a 31-Kda protein. *J. Magn. Reson.* **96:** 432–440.

Grzesiek, S., Anglister, J., and Bax, A. 1993. Correlation of backbone amide and aliphatic side-chain resonances in C-13/N-15–enriched proteins by isotropic mixing of C-13 magnetization. *J. Magn. Reson. B* **101:** 114–119.

Guntert, P., Mumenthaler, C., and Wuthrich, K. 1997. Torsion angle dynamics for NMR structure calculation with the new program DYANA. *J. Mol. Biol.* **273:** 283–298.

Huang, Y.P.J., Swapna, G.V.T., Rajan, P.K., Ke, H.P., Xia, B., Shukla, K., Inouye, M., and Montelione, G.T. 2003. Solution NMR structure of ribosome-binding factor A (RbfA), a cold-shock adaptation protein from *Escherichia coli*. *J. Mol. Biol.* **327:** 521–536.

Jacob, Y., Badrane, H., Ceccaldi, P.E., and Tordo, N. 2000. Cytoplasmic dynein LC8 interacts with lyssavirus phosphoprotein. *J. Virol.* **74:** 10217–10222.

Jaffrey, S.R. and Snyder, S.H. 1996. PIN: An associated protein inhibitor of neuronal nitric oxide synthase. *Science* **274:** 774–777.

Jones, S. and Thornton, J.M. 1995. Protein–protein interactions: A review of protein dimer structures. *Prog. Biophys. Mol. Biol.* **63:** 31–65.

King, S.M., Barbarese, E., Dillman, J.F., Benashski, S.E., Do, K.T., Patel-King, R.S., and Pfister, K.K. 1998. Cytoplasmic dynein contains a family of differentially expressed light chains. *Biochemistry* **37:** 15033–15041.

Koradi, R., Billeter, M., and Wuthrich, K. 1996. MOLMOL: A program for display and analysis of macromolecular structures. *J. Mol. Graph.* **14:** 51–55.

Kuboniwa, H., Grzesiek, S., Delaglio, F., and Bax, A. 1994. Measurement of H-N-H-α J couplings in calcium-free calmodulin using new 2D and 3D water-flip-back methods. *J. Biomol. NMR* **4:** 871–878.

Laskowski, R.A., Rullmann, J.A.C., MacArthur, M.W., Kaptein, R., and Thornton, J.M. 1996. AQUA and PROCHECK-NMR: Programs for checking the quality of protein structures solved by NMR. *J. Biomol. NMR* **8:** 477–486.

Liang, J., Edelsbrunner, H., Fu, P., Sudhakar, P.V., and Subramaniam, S. 1998. Analytical shape computation of macromolecules, I: Molecular area and volume through α shape. *Proteins* **33:** 1–17.

Liang, J., Jaffrey, S.R., Guo, W., Snyder, S.H., and Clardy, J. 1999. Structure of the PIN/LC8 dimer with a bound peptide. *Nat. Struct. Biol.* **6:** 735–740.

Makokha, M., Hare, M., Li, M., Hays, T., and Barbar, E. 2002. Interactions of cytoplasmic dynein light chains Tctex-1 and LC8 with the intermediate chain IC74. *Biochemistry* **41:** 4302–4311.

Moseley, H.N.B., Sahota, G., and Montelione, G.T. 2003. Assignment validation software suite for the evaluation and presentation of protein resonance assignment data. *J. Biomol. NMR* (in press).

Muhandiram, D.R. and Kay, L.E. 1994. Gradient-enhanced triple-resonance 3-dimensional NMR experiments with improved sensitivity. *J. Magn. Reson. B* **103:** 203–216.

Naisbitt, S., Valtschanoff, J., Allison, D.W., Sala, C., Kim, E., Craig, A.M., Weinberg, R.J., and Sheng, M. 2000. Interaction of the postsynaptic density-95/guanylate kinase domain-associated protein complex with a light chain of myosin-V and dynein. *J. Neurosci.* **20:** 4524–4534.

Nyarko, A., Hare, M., Makokha, M., and Barbar, E. 2003. Interactions of LC8 with N-terminal segments of the intermediate chain of cytoplasmic dynein. *Sci. World J.* **3:** 647–654.

Pascal, S.M., Muhandiram, D.R., Yamazaki, T., Forman-Kay, J.D., and Kay, L.E. 1994. Simultaneous acquisition of N-15– and C-13–edited NOE spectra of proteins dissolved in H_2O. *J. Magn. Reson. B* **103:** 197–201.

Puthalakath, H., Huang, D.C.S., O'Reilly, L.A., King, S.M., and Strasser, A. 1999. The proapoptotic activity of the Bcl-2 family member Bim is regulated by interaction with the dynein motor complex. *Mol. Cell* **3:** 287–296.

Raux, H., Flamand, A., and Blondel, D. 2000. Interaction of the rabies virus P protein with the LC8 dynein light chain. *J. Virol.* **74:** 10212–10216.

Richardson, J.S. and Richardson, D.C. 2002. Natural β-sheet proteins use negative design to avoid edge-to-edge aggregation. *Proc. Natl. Acad. Sci.* **99:** 2754–2759.

Rodriguez-Crespo, I., Straub, W., Gavilanes, F., and de Montellano, P.R.O. 1998. Binding of dynein light chain (PIN) to neuronal nitric oxide synthase in the absence of inhibition. *Arch. Biochem. Biophys.* **359:** 297–304.

Schlunegger, M.P., Bennett, M.J., and Eisenberg, D. 1997. Oligomer formation by 3D domain swapping: A model for protein assembly and misassembly. *Adv. Protein Chem.* **50:** 61–122.

Schnorrer, F., Bohmann, K., and Nusslein-Volhard, C. 2000. The molecular motor dynein is involved in targeting swallow and bicoid RNA to the anterior pole of *Drosophila* oocytes. *Nat. Cell Biol.* **2:** 185–190.

Tochio, H., Ohki, S., Zhang, Q., Li, M., and Zhang, M.J. 1998. Solution structure of a protein inhibitor of neuronal nitric oxide synthase. *Nat. Struct. Biol.* **5:** 965–969.

Wang, W., Lo, K.W.-H., Kan, H., Fan, J., and Zhang, M. 2003. Structure of the monomeric 8-kd dynein light chain and mechanism of the domain swapped dimer assembly. *J. Biol. Chem.* **278:** 41491–41499.

Xu, D., Tsai, C.J., and Nussinov, R. 1998. Mechanism and evolution of protein dimerization. *Protein Sci.* **7:** 533–544.

Zimmerman, D.E., Kulikowski, C.A., Huang, Y.P., Feng, W.Q., Tashiro, M., Shimotakahara, S., Chien, C.Y., Powers, R., and Montelione, G.T. 1997. Automated analysis of protein NMR assignments using methods from artificial intelligence. *J. Mol. Biol.* **269:** 592–610.